Journal of Power Sources 232 (2013) 181–186

Contents lists available at SciVerse ScienceDirect

Journal of Power Sources

journal homepage: www.elsevier.com/locate/jpowsour

Short communication

Excellent rate capabilities of ($LiFePO_4$/C)//LiV_3O_8 in an optimized aqueous solution electrolyte

Mingshu Zhao*,[1], Bao Zhang, Guanliang Huang, Hanyuan Zhang, Xiaoping Song

MOE Key Laboratory for Non-equilibrium Synthesis and Modulation of Condensed Matter, School of Science, Xi'an Jiaotong University, Xi'an 710049, China

HIGHLIGHTS

- The optimized aqueous electrolyte (OAE) is 9 M $LiNO_3$ solution without oxygen.
- LiV_3O_8//($LiFePO_4$/C) presents good cycling performance in the OAE.
- This ARLB has large capacity at higher *C*-rate such as 30*C* and 50*C*.

GRAPHICAL ABSTRACT

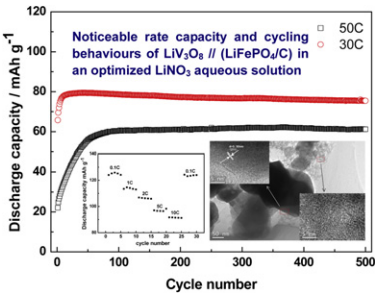

ARTICLE INFO

Article history:
Received 25 October 2012
Received in revised form
2 January 2013
Accepted 3 January 2013
Available online 16 January 2013

Keywords:
Lithium ferrous phosphates
Aqueous rechargeable lithium-ion battery
Optimized electrolyte
Rate performance

ABSTRACT

$LiFePO_4$/C composites prepared by the hydrothermal method and the calcinations process are used as the cathode material for ARLBs. The ARLB is built up with $LiFePO_4$/C and LiV_3O_8 in 9 M $LiNO_3$ aqueous electrolyte without the dissolved oxygen, which can deliver a capacity of 88.7 mAh g^{-1} at 10*C*-rate after 100 cycles. This ARLB has still the discharge capacity of 60 mAh g^{-1} at 50*C*-rate after 500 cycles. The excellent rate capabilities show that this ARLB exhibits great potential as the power sources for high power applications.

1. Introduction

Lithium-ion batteries (LIBs) have been extensively used in powering portable devices. Unfortunately, their safety and high cost limits their application for large scale energy storage because LIBs use the flammable and expensive organic electrolytes. An aqueous rechargeable lithium battery (ARLB) was first reported by Dahn et al., which has advantages such as safety and low cost [1–6].

Currently researches surrounding cathodes for ARLBs, including $LiCoO_2$ [7–12], $LiMn_2O_4$ [13–17], $LiMePO_4$ (Me = Co, Ni, Fe) [18–22] and $LiFePO_4$ [23–28] are underway. Thereinto, Mi et al. studied the electrochemical behaviors of solid $LiFePO_4$ in Li_2SO_4 aqueous electrolyte [25]. Minakshi reported Li^+ intercalation into amorphous $FePO_4$ cathode in an aqueous solution [26]. Lee et al. researched the electrochemical properties of $LiFePO_4$ in different pH aqueous electrolyte [27]. Xia et al. investigated the capacity fading of $LiFePO_4$ in an aqueous electrolyte [24]. However, they seldom mentioned how to improve the rate capability of $LiFePO_4$ in an aqueous electrolyte. Fortunately, Wu et al. studied the rate capability of $LiMn_2O_4$ in the aqueous electrolyte and obtained ARLBs with good cycling behaviors [29,30]. Table 1 gives the

* Corresponding author. Tel.: +86 029 82663034.
E-mail address: zhaomshu@mail.xjtu.edu.cn (M. Zhao).
[1] ISE (International Society of Electrochemistry) member.

0378-7753/$ – see front matter © 2013 Elsevier B.V. All rights reserved.
http://dx.doi.org/10.1016/j.jpowsour.2013.01.026

Table 1
Electrochemical properties of different cathode active materials in various aqueous electrolytes.

Cathode materials	Electrolyte solution	Theoretical capacity (mAh g^{-1})	Capacity in the 1st cycle (mAh g^{-1})	Capacity in the n^{th} cycles (mAh g^{-1})	Current density or C_{rate}	Capacity retention (%)	References
$LiCoO_2$	Saturated $LiNO_3$	140	60	45 (12)	0.2 mA cm^{-2}	75%	[7]
$LiCoO_2$	1 M $LiNO_3$	140	105	95 (90)	1*C*	90%	[9]
$LiCoO_2$	0.5 M Li_2SO_4	140	143	143 (40)	1000 mA g^{-1}	No evident capacity fading	[10]
			133	133 (40)	10,000 mA g^{-1} (70*C*)	No evident capacity fading	
$LiCoO_2$	2 M $LiNO_3$	140	115	105 (50)	25 mA g^{-1}	91%	[11]
$LiCoO_2$	Saturated Li_2SO_4	140	47.7	47.7 (120)	0.1*C*	No evident capacity fading	[12]
$LiMn_2O_4$	5 M $LiNO_3$	148	43	35 (60)	0.2*C*	81%	[13]
$LiMn_2O_4$	5 M $LiNO_3$	148	110	100 (56)	10*C*	91%	[14]
$LiMn_2O_4$	Saturated $LiNO_3$	148	127	110 (24) 100 (42)	0.2*C*	92% 83%	[15]
$LiMn_2O_4$	5 M $LiNO_3$	148	118	103 (40)	0.2*C*	87%	[16]
$LiMn_2O_4$	0.5 M Li_2SO_4	148	118	110 (10,000)	90*C*	93%	[29]
$LiMn_2O_4$	0.5 M Li_2SO_4	148	120	92 (150)	500 mA g^{-1}	77%	[30]
$LiCoPO_4$	Saturated LiOH	167	82	70 (25)	0.5 mA cm^{-2}	85%	[18]
$LiNiPO_4$	Saturated LiOH	167	55	50 (25)	0.5 mA cm^{-2}	90%	[19]
$LiFe_{0.5}Mn_{0.5}PO_4$	LiOH + saturated $LiNO_3$	167	67	54 (80)	50*C*	81%	[20]
$LiMn_{0.05}Ni_{0.05}Fe_{0.9}PO_4$	Saturated Li_2SO_4	167	104	55 (50)	0.2 mA cm^{-2}	53%	[21]
$LiFePO_4$	1 M Li_2SO_4	170	55(1C)	–	6*C*	90%(1000)	[23]
$LiFePO_4$	(0.5 M Li_2SO_4) + LiOH	170	130	82 (10)	0.2*C*	63%	[24]
$LiFePO_4$	**9 M $LiNO_3$**	**170**	**90**	**88.7 (100)**	**10C**	**99%**	**In this paper**

discharge capacity and the capacity retention comparisons among different cathode materials in various aqueous electrolyte solutions used for ARLBs, and it also lists the electrochemical capacities in this paper. It is well known that the anode materials are also key component of the ARLB. Up to now, LiV_3O_8 is one of the most hopeful anode materials used for the ARLB, and the references reported its preparation, corresponding electrochemical performance and Li^+ intercalation/de-intercalation mechanism [31–34]. In this paper, we also select LiV_3O_8 performed as the anode active material for the ARLB system, and it was synthesized by multiple sinter method [35], which is different from that reported in ref. [36].

Here, we report our findings to provide a significant approach to improve $LiFePO_4$'s comprehensive performances for the ARLBs in the practical applications. LiV_3O_8//($LiFePO_4$/C) ARLBs in an optimized $LiNO_3$ solution were assembled, and the rate capabilities were studied, especially the cycling behaviors at high *C*-rate, such as 30*C* and 50*C*.

2. Experimental

$CH_3COOLi{\cdot}2H_2O$, $Fe(NO_3)_3{\cdot}9H_2O$, and $NH_4H_2PO_4$ with a molar ratio of 1:1:1 were dissolved in 30 mL distilled water under magnetic stirring; then 2.5 mL ethylene glycol (EG) was added to the blend solution to adjust its pH value equal to 1. After stirring 15 min, 2 mL anhydrous ethylenediamine (EN) was added to the solution dropwise until pH = 8. Upon the addition of EN, the solution becomes a stiff gel. The color of the gelatinous mixture finally becomes orange with continuous stirring for 30 min. This solution was transferred into a 50 mL Teflon autoclave. The autoclave was sealed, kept at 180 °C for 3 h in an electric oven, and then cooled to room temperature naturally. The above substance was heated in an evaporation pan at 80 °C under stirring to get a black brown precursor. The precursor and 0.198 g sucrose were mixed to press a pellet, and calcined at 700 °C for 12 h in the purified argon gas flowing to obtain $LiFePO_4$/C composites. LiV_3O_8 was synthesized as describe in ref [15].

The sample was characterized by XRD analysis using Bruker D8-Adavanced diffractometer with Cu K*a* radiation. The morphologies were observed by JEOL JEM-2100. The residual carbon weight percentage was measured using the thermo-gravimetry (TG).

The working electrode (WE) was fabricated with the as-prepared materials, acetylene black and polyvinylidene fluoride (PVDF) with a weight ratio of 80:10:10 using N-methylpyrrolidone as solvent, the black slurry was uniform mixed with ultrasonic process for about 2 min, then coated on a nickel mesh followed by drying at 373 K for 10 h under vacuum. The counter electrode (CE) was described as the same as in ref. [16]. The saturated calomel electrode (0.242 *vs.* SHE/V) was used as the reference electrode (RE). The ARLB was built up with WE, CE and RE in the different concentration of $LiNO_3$ aqueous solution which was prepared by bubbling high-purity nitrogen for 3 h. The galvanostatic charge–discharge tests within the voltage range of 0 V–0.8 V (*vs.* SCE) and the rate capability from 0.1*C* to 50*C*-rate were performed using Arbin BT2000 instrument. The cyclic voltammetry (CV) curves at 5 mV s^{-1} within −0.2 V–0.8 V (*vs.* SCE) were recorded by Ametek VMC-4.

3. Results and discussion

The XRD pattern of the synthesized $LiFePO_4$/C composite is shown in Fig. 1a. $LiFePO_4$/C exhibit a crystalline orthorhombic structure (ICDD number: 01-010-6684), which has the typical crystal face index of the diffraction peaks such as (101), (111), (211), (311). The inset image of Fig. 1a is the electron diffraction pattern of $LiFePO_4$/C, which indicates that the particle is composed of many smaller crystallites. Fig. 1b illustrates the SEM image of $LiFePO_4$/C and the morphology of the particles present oval shape, which are connected with the mesh carbon. HRTEM micrographs (Fig. 1c) of the nano-composite particles show the spacing of lattice fringes along the direction is 0.30 nm, which corresponds to {211} crystal plane of olivine $LiFePO_4$.

The CV curves of $LiFePO_4$/C electrode in $LiNO_3$ aqueous electrolyte at the scan rate of 5 mV S^{-1} for 10 cycles between −0.2 V and 0.8 V (*vs.* SCE) are shown in Fig. 2a. The anodic/cathodic peak

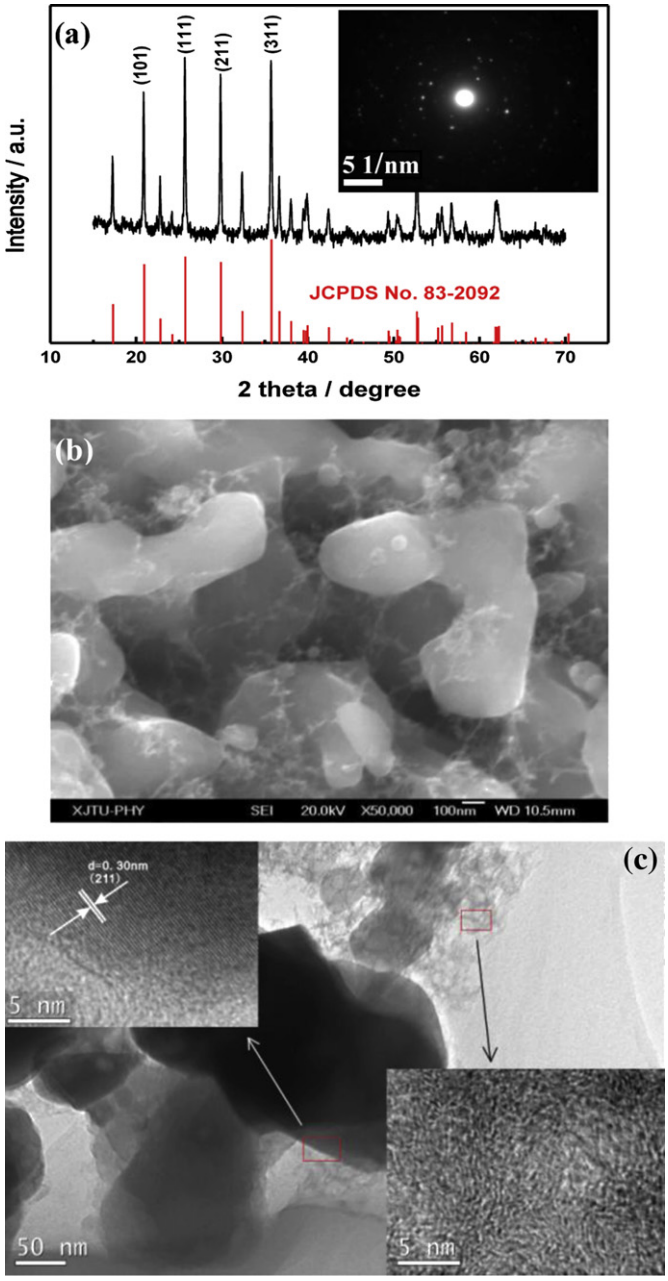

Fig. 1. Characteristics of $LiFePO_4$/C composites. (a) XRD patterns, inset image: ED patterns. (b) SEM images. (c) TEM images, inset images: HRTEM photos of the given area.

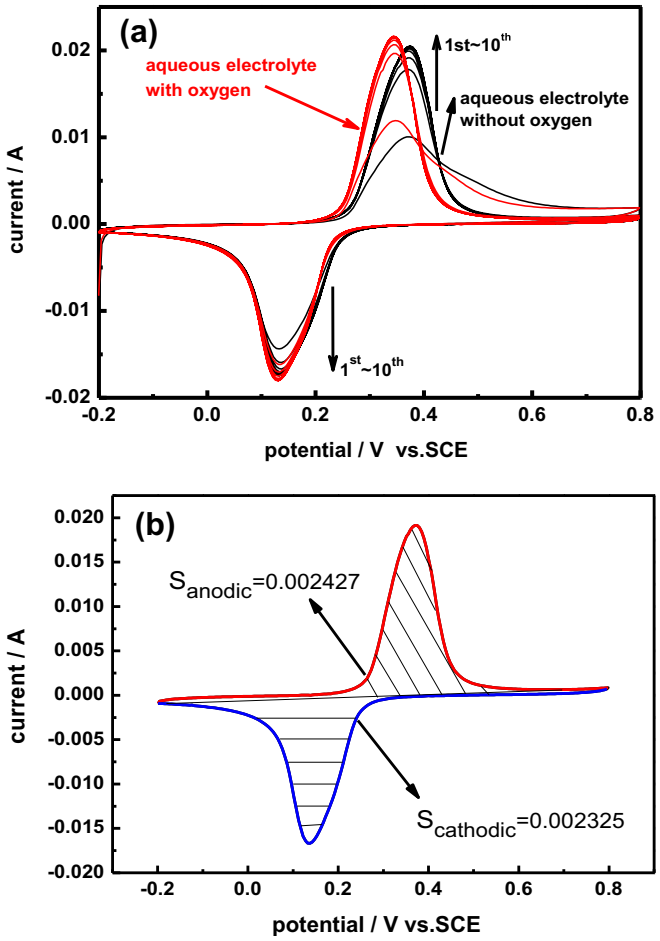

Fig. 2. CV curves of $LiFePO_4$/C in the aqueous electrolyte with/without the dissolved oxygen at 5 mV s^{-1}. (a) CV curves of 10 cycles. (b) Schematic diagram of CV curve for the calculation.

situated at 0.35/0.13 V (*vs.* SCE) and 0.38/0.13 V (*vs.* SCE) for $LiFePO_4$/C in the aqueous electrolyte with or without the dissolved oxygen at the first cycle, respectively, which correspond to the reversible insertion/extraction of lithium ions into/from $LiFePO_4$/C. After 10 cycles, the anodic/cathodic peaks are situated at 0.32/0.13 V (*vs.* SCE) and 0.38/0.13 V (*vs.* SCE), which are also consistent with the intercalation/deintercalation of lithium ions into/from the host olivine structure of $LiFePO_4$/C. This means that $LiFePO_4$/C composites will present good reversibility of lithium ions insertion/extraction. At the same scan rate, the potential difference between the redox peaks of $LiFePO_4$/C in the aqueous electrolyte with the dissolved oxygen is smaller than that in the aqueous electrolyte without the dissolved oxygen, which indicates that the removal of the dissolved oxygen from the aqueous electrolyte made the reversibility of $LiFePO_4$/C increase. Therefore, we could apply the integral area ratio of reduction/oxidation peak to judge the intercalation/deintercalation reversibility of Li^+. Fig. 2b illustrates a schematic diagram of the integral area ratio of reduction/oxidation peak for $LiFePO_4$/C electrode in the aqueous electrolyte without the dissolved oxygen at the 3rd cycle and the ratio is about 0.958, which is higher than that value (0.935) of $LiFePO_4$/C electrode in the aqueous electrolyte with the dissolved oxygen. The results demonstrate that the value is much closer to 1, much more reversible of the lithium ions insertion/extraction into/from $LiFePO_4$/C intrinsic structure. Thus, the removal of the dissolved oxygen from the aqueous electrolyte is beneficial to the reversibility of lithium ions into/from the olivine $LiFePO_4$/C cathode materials.

The cycling behaviors of LiV_3O_8/$LiNO_3$/($LiFePO_4$/C) ARLBs at 1*C*-rate are shown in Fig. 3a. This ARLB exhibits an improved cycling performance in $LiNO_3$ without the dissolved oxygen compared with that with the dissolved oxygen. The first discharge capacity of the former is about 110 mAh g^{-1}, and it remains this capacity until 100 cycles, which has nearly no loss. However, the latter is about 100 mAh g^{-1}, and it only has 70 mAh g^{-1} after 100 cycles, which displays a rapid capacity fading after 50 cycles. It is proofed that the removal of the dissolved oxygen from the aqueous electrolyte can inhibit the side reaction for the ARLB during the redox reactions process. In the inset image of Fig. 3a, it illustrates the 3rd charge–discharge curves of the ARLBs with/without the dissolved oxygen in

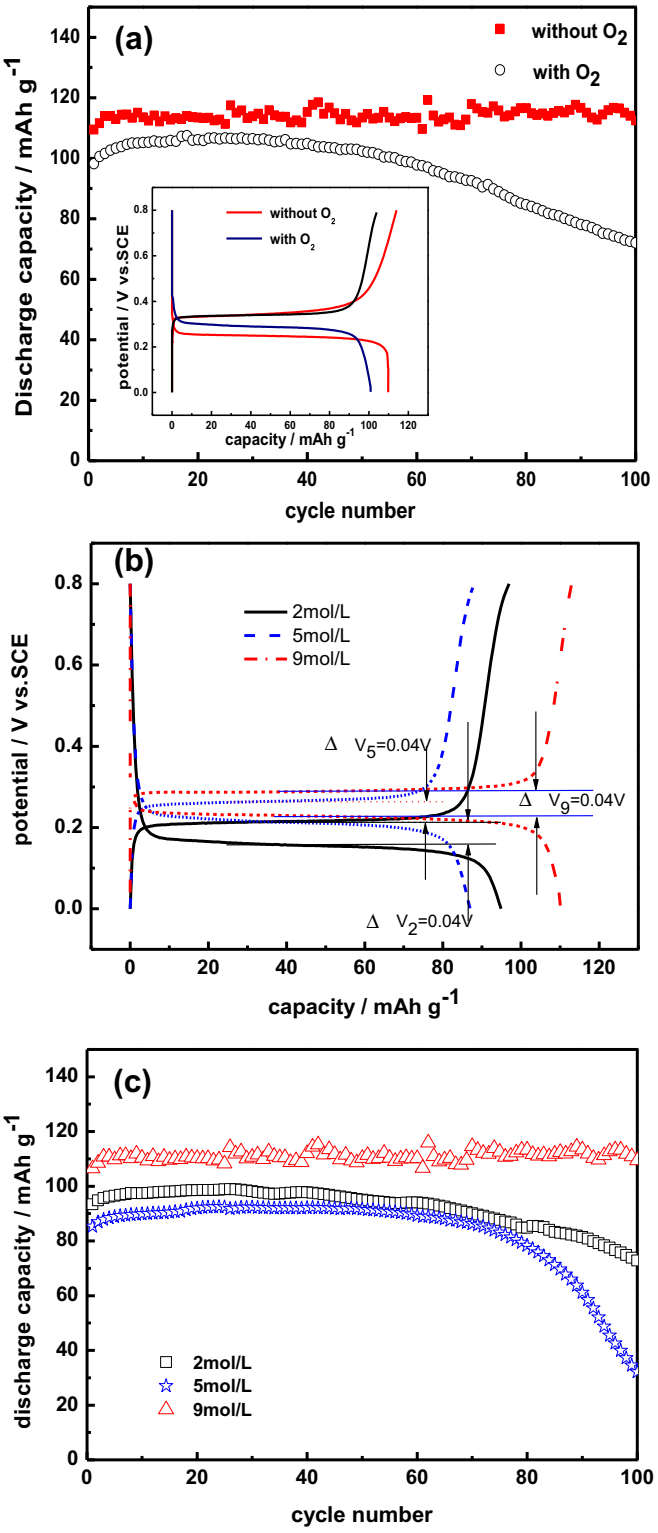

Fig. 3. Electrochemical performances of ($LiFePO_4$/C)//LiV_3O_8 ARLB in the optimized aqueous electrolyte. (a) Cycling behaviors of ARLB in the aqueous electrolyte with/without the dissolved oxygen, inset image: the 3rd charge–discharge curves of ARLB with/without the dissolved oxygen. (b) The 2nd charge–discharge curves at 1*C*-rate of ARLB in different concentration of $LiNO_3$ solution without the dissolved oxygen. (c) Cycling behaviors of ARLB in different concentration of $LiNO_3$ solution without the dissolved oxygen.

the aqueous solution, and there is an evident plateau, indicating clearly the redox reactions of $LiFePO_4$. It is notable that the voltage difference of the charge–discharge voltage plateau for the ARLB with the dissolved oxygen is smaller than that of the ARLB without the dissolved oxygen, which is consistent with CV results. These results suggest that the ARLB without the dissolved oxygen presents the better cycling behavior, which is due to smaller electrochemical resistance and less polarization of the optimized aqueous electrolyte, and the results are also consistent to the reported studies in ref. [23].

Fig. 3b and c shows the 3rd charge–discharge curves and the cycling behaviors of the ARLBs in different concentration of $LiNO_3$ solution without the dissolved oxygen at 1*C*-rate. In Fig. 3b, the charge/discharge voltage plateau of the ARLBs in 2 M, 5 M and 9 M $LiNO_3$ solution is 0.21 V/0.17 V, 0.26 V/0.21 V and 0.29 V/0.25 V, respectively. Although the ARLBs in various concentration of the aqueous electrolyte, the potential differences (noted as ΔV) between the charge–discharge voltage plateau are the same, i.e. $\Delta V = 0.04$ V. It is known that the potential difference between the charge–discharge voltage plateaus is related to the polarization of the electrode materials and the voltage lag [37]. It can be observed from Fig. 3b that the value of the charge/discharge voltage plateau is enhanced with the increased concentration of $LiNO_3$ solution, however, the potential difference between the charge–discharge voltage plateau is not changed, which indicates that the concentration of the aqueous solution has little effects on the polarization of the electrode materials and the voltage lag. In addition, the 1st discharge capacity of the ARLB in 2 M, 5 M and 9 M $LiNO_3$ is 93 mAh g^{-1}, 85 mAh g^{-1}, 108 mAh g^{-1}, respectively, and after 100 cycles, the ARLB displays a discharge capacity of 75 mAh g^{-1}, 30 mAh g^{-1}, 110 mAh g^{-1}, separately. These results appear that ARLB in 9 M $LiNO_3$ has the best cycling behaviors at 1*C*-rate. It is unclear why the capacity of the cell containing 5 M $LiNO_3$ exhibits the lowest capacity. A deeper investigation is underway.

The rate performances of the ARLBs in the optimized aqueous electrolyte are shown in Fig. 4. In Fig. 4a, the ARLBs display the 1st discharge capacity of 123 mAh g^{-1}, 110 mAh g^{-1}, 104 mAh g^{-1}, 98 mAh g^{-1}, 90 mAh g^{-1} at 0.1*C*, 1*C*, 2*C*, 5*C*, 10*C*-rate, respectively. After 5 cycles at the following *C*-rate, 0.1*C*, 1*C*, 2*C*, 5*C*, 10*C*-rate, and its discharge capacity has no loss. Then the ARLB recycles at 0.1*C*-rate for 5 cycles again, the capacity still remains 123 mAh g^{-1}. These results demonstrate that this ARLB has good rate performance. In Fig. 4b, when the ARLB cycles at 1*C*, 2*C*, 5*C*, 10*C*-rate, the capacity is 109.4 mAh g^{-1}, 93.5 mAh g^{-1}, 85.8 mAh g^{-1}, 82.6 mAh g^{-1}, respectively, and after 100 cycles, the corresponding capacity is 112.5 mAh g^{-1}, 98.1 mAh g^{-1}, 90.1 mAh g^{-1}, 88.7 mAh g^{-1}, which show better cycling behaviors. Especially in Fig. 4c, while the ARLB recycles at higher discharge *C*-rate, such as 20*C*, 30*C*, 40*C* and 50*C*, it still has the capacity of 80 mAh g^{-1}, 76.6 mAh g^{-1}, 70 mAh g^{-1}, 60.8 mAh g^{-1} after 200 cycles. In Fig. 4d, it is noted that this ARLB has the discharge capacity of 73 mAh $g^{-1}$and 60 mAh g^{-1} at 30*C* and 50*C*-rate after 500 cycles. We found that the discharge capacity increases at the first ten cycles, and then remains stable at the following cycles until 500 cycles, while at 50*C*-rate, the discharge capacity increases at the first 80 cycles, and then remains much more stable at the following cycles until 500 cycles, which indicate that there exist the activation processes such as the activation of the electrode materials and the interface stability between the aqueous electrolyte and the electrode materials. These results are quite attractive attentions compared with the reported cycling performance of the ARLB [23–25,28].

Here, the ARLB fabricated with $LiFePO_4$/C and LiV_3O_8 in 9 M $LiNO_3$ aqueous solution without the dissolved oxygen exhibits excellent rate capabilities and good cycling behaviors. We can attribute these to the following reasons: (1) The as-prepared

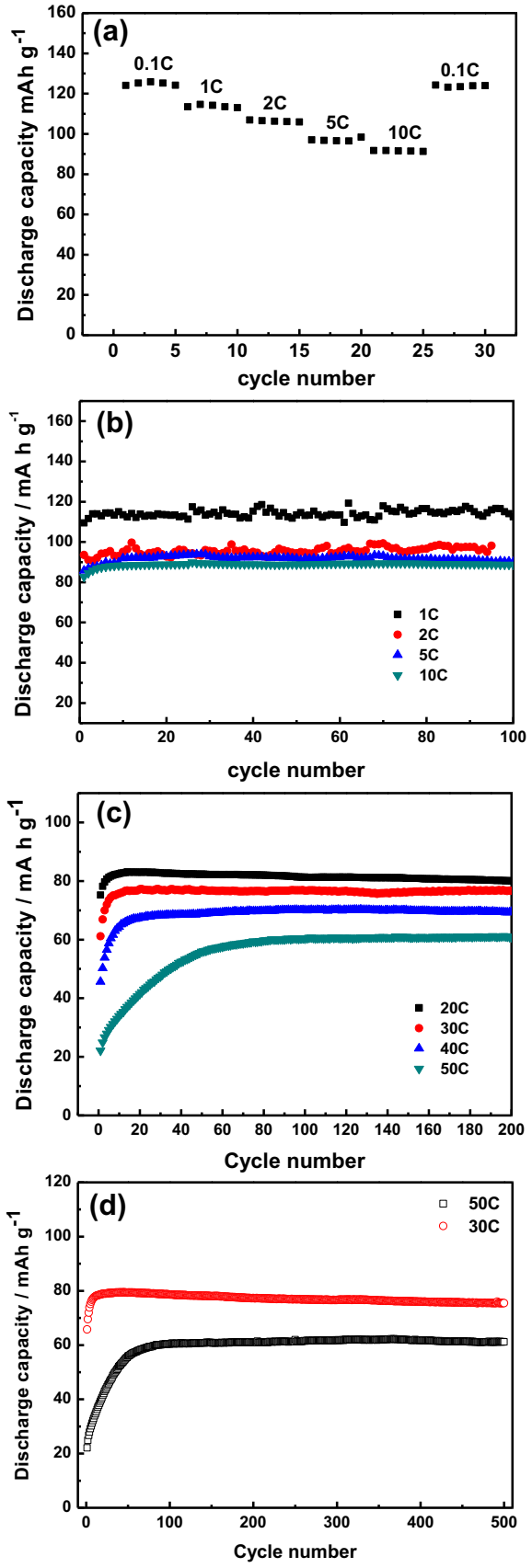

Fig. 4. Rate capability of ($LiFePO_4$/C)//LiV_3O_8 in 9 M $LiNO_3$ solution without the dissolved oxygen. (a) Five cycles at the following each *C*-rate such as 0.1*C*, 1*C*, 2*C*, 5*C*, 10*C* and undergo five cycles at 0.1*C*-rate again. (b) 100 cycles at 1*C*, 2*C*, 5*C*, 10*C*-rate. (c) 200 cycles at 20*C*, 30*C*, 40*C*, 50*C*-rate. (d) 500 cycles at 30*C* and 50*C*-rate.

cathode materials possess fine crystal particles of $LiFePO_4$, which are connected with the nanonet structure of the carbon, and this structure provides larger specific surface area, benefitting lithium ions to insert or extract from the host easily and quickly within the shorter time and improving the charge–discharge performance. (2) The optimized aqueous solution electrolyte has higher conductivity, which guarantees lithium ions to response quickly at higher *C*-rate.

4. Conclusions

Here report the optimized aqueous electrolyte is introduced to improve the rate performance of the ARLB system. This ARLB is fabricated with $LiFePO_4$/C and LiV_3O_8 in 9 M $LiNO_3$ aqueous solution without the dissolved oxygen. This ARLB displays not only good cycling performance but also well rate capability. Even at 50C-rate, after 500 cycles, the ARLB has still discharge capacity of 60 mAh g^{-1}. These excellent performances indicate that this battery will be applied for the high power devices and the stored energy.

Acknowledgments

The authors acknowledge the Province Natural Science Foundation of Shaan Xi (2012JM6005), Xi'an Science and Technology project (CXY1124), and the China Fundamental Research Funds for the Central University (xjj2012095, 2012jdh235 and SPCW006476).

Appendix A. Supplementary data

Supplementary data related to this article can be found at http://dx.doi.org/10.1016/j.jpowsour.2013.01.026.

References

[1] W. Li, J.R. Dahn, D.S. Wainwright, Science 264 (1994) 1115.
[2] W. Li, W.R. Mckinnon, J.R. Dahn, J. Electrochem. Soc. 141 (1994) 2310.
[3] W. Li, J.R. Dahn, J. Electrochem. Soc. 142 (1995) 1742.
[4] Y.G. Wang, Y.Y. Xia, Electrochem. Commun. 7 (2005) 1138.
[5] G.J. Wang, L.J. Fu, N.H. Zhao, L.C. Yang, Y.P. Wu, H.Q. Wu, Angew. Chem. Int. Ed. 46 (2007) 295.
[6] J.Y. Luo, Y.Y. Xia, Adv. Funct. Mater. 17 (2007) 3877.
[7] G.J. Wang, N.H. Zhao, L.C. Yang, Y.P. Wu, H.Q. Wu, R. Holze, Electrochim. Acta 52 (2007) 4911.
[8] G.J. Wang, Q.T. Qu, B. Wang, Y. Shi, S. Tian, Y.P. Wu, R. Holze, Electrochim. Acta 54 (2009) 1199.
[9] R. Ruffo, C. Wessells, R.A. Huggins, Y. Cui, Electrochem. Commun. 11 (2009) 247.
[10] W. Tang, L.L. Liu, S. Tian, L. Li, Y.B. Yue, Y.P. Wu, S.Y. Guan, K. Zhu, Electrochem. Commun. 12 (2010) 1524.
[11] X.L. Zeng, Y.Y. Huang, F.L. Luo, Y.B. He, D.G. Tong, J. Sol–Gel Sci. Technol. 54 (2010) 139.
[12] G.J. Wang, L.C. Yang, Q.T. Qu, B. Wang, Y.P. Wu, R. Holze, J. Solid State Electrochem. 14 (2010) 865.
[13] H.B. Wang, Y.Q. Zeng, K.L. Huang, S.Q. Liu, L.Q. Chen, Electrochim. Acta 52 (2007) 5102.
[14] M. Zhao, X. Song, F. Wang, W. Dai, X. Lu, Electrochim. Acta 56 (2011) 5673.
[15] M. Zhao, Q. Zheng, F. Wang, W. Dai, X. Song, Electrochim. Acta 56 (2011) 3781.
[16] M. Zhao, B. Zhang, G. Huang, W. Dai, F. Wang, X. Song, Energy & Fuels 26 (2012) 1214.
[17] M. Jayalakshmi, M.M. Rao, F. Scholz, Langmuir 19 (2003) 8403.
[18] M. Minakshi, P. Singh, N. Sharma, M. Blackford, M. Ionescu, Ind. Eng. Chem. Res. 50 (2011) 1899.
[19] M. Minakshi, P. Singh, D. Appadoo, D.E. Martin, Electrochim. Acta 56 (2011) 4356.
[20] M. Zhao, G. Huang, B. Zhang, F. Wang, X. Song, J. Power Sources 211 (2012) 202.
[21] X.H. Liu, T. Saito, T. Doi, S. Okada, J. Yamaki, J. Power Sources 189 (2009) 706.
[22] M. Minakshi, N. Sharma, D. Ralph, D. Appadoo, K. Nallathamby, Electrochem. Solid-State Lett. 14 (2011) A86.
[23] J.Y. Luo, W.J. Cui, P. He, Y.Y. Xia, Nat. Chem. 2 (2010) 760.
[24] P. He, J.L. Liu, W.J. Cui, J.Y. Luo, Y.Y. Xia, Electrochim. Acta 56 (2011) 2351.
[25] C.H. Mi, X.G. Zhang, H.L. Li, J. Electroanal. Chem. 602 (2007) 245.
[26] M. Minakshi, Electrochim. Acta 55 (2010) 9174.
[27] J.H. Lee, H.H. Kim, G.S. Kim, D.S. Zang, Y.M. Choi, H. Kim, D.K. Yi, W.M. Sigmund, U. Paik, J. Phys. Chem. C114 (2010) 4466.

[28] H. Manjunatha, G.S. Suresh, T.V. Venkatesha, J. Solid State Electrochem. 15 (2011) 431.
[29] Q. Qu, L. Fu, X. Zhan, D. Samuelis, J. Maier, L. Li, S. Tian, L. Li, Y. Wu, Energy Environ. Sci. 4 (2011) 3985.
[30] W. Tang, L. Liu, Y. Zhu, H. Sun, Y. Wu, K. Zhu, Energy Environ. Sci. 5 (2012) 6909.
[31] J. Köhler, H. Makihara, H. Uegaito, H. Inoue, M. Toki, Electrochim. Acta 46 (2000) 59.
[32] C. Cheng, Z.H. Li, X.Y. Zhan, Q.Z. Xiao, G.T. Lei, X.D. Zhou, Electrochim. Acta 55 (2010) 4627.
[33] A. Caballero, J. Morales, O. Vargas, J. Power Sources 195 (2010) 4318.
[34] G.J. Wang, Q.T. Qu, B. Wang, Y. Shi, S. Tian, Y.P. Wu, R. Holze, J. Power Sources 189 (2009) 503.
[35] M. Zhao, Q. Zheng, F. Wang, W. Dai, K. Peng, X. Song, Preparation of an Inorganic Aqueous Electrolyte Solution Lithium Ion Rechargeable Battery System, CN 101656329A, 20100224.
[36] S. Jouanneau, A.L. La Salle, A. Verbaere, M. Deschamps, S. Lascaud, D. Guyomard, J. Mater. Chem. 13 (2003) 921.
[37] W. Dreyer, J. Jamnik, C. Guhlke, R. Huth, J. Moškon, M. Gaberšcek, Nat. Mater. 9 (2010) 448.